

# Understanding the Effectiveness of Phospholane Electrolyte Additives in Lithium-Ion Batteries under High-Voltage Conditions

Christian Wölke<sup>+</sup>,<sup>[a]</sup> Diddo Diddens<sup>+</sup>,<sup>[a]</sup> Bastian Heidrich,<sup>[b]</sup> Martin Winter,<sup>[a, b]</sup> and Isidora Cekic-Laskovic<sup>\*[a]</sup>

Six phospholane functional electrolyte additives that enable the formation of an effective cathode electrolyte interphase (CEI) via a polymerization reaction on the electrode surface were designed, synthesized, and comparatively analyzed by means of complementary experimental and computational methods in order to understand their mode of action in NMC111||graphite battery cells under high voltage conditions. Two reaction mechanisms, namely a phosphate-based and a phosphonate-based mechanism, were postulated and, based on systematic

analysis, the phosphate mechanism was identified as the more likely. Direct correlation of the phospholane's structural features and relevant properties impacting the direct correlation of the phospholane's structural features and relevant properties impacting the overall cycling performance of NMC111||graphite cells, as depicted by capacity retention, stands for a vital example approach towards identifying promising electrolyte components for advanced, targeted applications.

## 1. Introduction

The invention of the lithium ion battery with its unmatched energy density laid the foundation of our modern, connected society where portable electronics have become an integral part of everyday life.[1,2] At the same time, the lithium ion battery pushed the available energy densities of energy storage systems to an area where electric vehicles become feasible and thus is an important driving force for the transition to a more sustainable energy consumption.[3,4] The rising demand for consumer grade portable electronics as well as electric vehicles generates a strong drive for the development of batteries with enhanced cycle life and higher energy densities than state of the art devices. While the development of novel electrode materials with higher specific capacities can significantly raise available energy densities, [5,6] changes on the large scales of industrial battery production are only reluctantly made once supply chains and processes are in place.[7] Introduction of functional additives to already established electrolyte formulations in order to increase the cell's safety, cycle life or the operating voltage and thus the achievable energy density stands for one of the most effective and cost affordable approaches.<sup>[8-10]</sup> The advantage in the latter approach is that the simple and cost effective implementation into existing processes enables tailoring of vital electrolyte properties for targeted requirements.

Since liquid battery electrolytes are multi-component systems, the number of possible electrolyte formulations is virtually unlimited.[11-14] At the same time, the number of possible chemical structures for each functional additive class is equally large. Therefore, identifying the "best" functional additive for a given battery electrolyte can be as the proverbial search for the needle in the haystack. However, if we understand the fundamental properties of both the electrolyte and battery cell system, we can significantly reduce the haystack's size and thus accelerate the search toward identification of "the right needle". Following this line of thought, we analyzed the proposed working mechanism of phospholane functional additives<sup>[15,16]</sup> by means of density-functional theory (DFT) calculations and chemical reasoning and designed a series of phospholane molecules featuring small, systematic changes to their structure (Figure 1). The proposed functional additives were synthesized (3,3,3-trifluoro-n-propylethylene-phosphite (TFnPrEPi) actually for the first time) and each structure's impact on the overall cycling performance of NMC111||graphite cells was studied.

### [a] Dr. C. Wölke,\* Dr. D. Diddens,\* Prof. Dr. M. Winter, Dr. I. Cekic-Laskovic Helmholtz-Institute Münster (IEK-12) Forschungszentrum Jülich GmbH Corrensstrasse 46, 48149 Münster, Germany E-mail: i.cekic-laskovic@fz-juelich.de

[b] B. Heidrich, Prof. Dr. M. Winter MEET Battery Research Center University of Münster Corrensstrasse 46, 48149 Münster, Germany

[+] These authors contributed equally to this work.

Supporting information for this article is available on the WWW under https://doi.org/10.1002/celc.202100107

© 2021 The Authors. ChemElectroChem published by Wiley-VCH GmbH. This is an open access article under the terms of the Creative Commons Attribution License, which permits use, distribution and reproduction in any medium, provided the original work is properly cited.

### 2. Results and Discussion

It has been previously proposed that the beneficial effect of phospholane functional additives stems from the formation of an effective cathode electrolyte interphase (CEI)<sup>[17]</sup> layer by means of a polymerization reaction on the cathode surface

Figure 1. Chemical structures of considered phospholane additives: npropylethylenephosphite (nPrEPi), iso-propylethylenephosphite (iPrEPi), tertbutylethylenephosphite (tBuEPi), 3,3,3-trifluoro-n-propylethylene-phosphite (TFnPrEPi), hexafluoro-iso-propylethylenephosphite (HFiPrEPi), and nonafluoro-tert-butylethylenephosphite (NFtBuEPi).

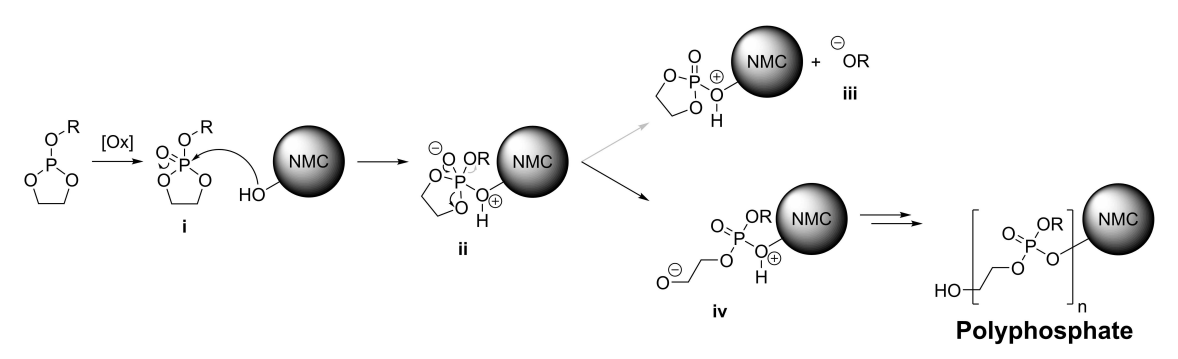
(Scheme 1).[15,16,18] In the first step, the phospholane molecule is oxidized to the corresponding phosphate i.[19] which makes it susceptible to a nucleophilic attack of a hydroxy group from the active material surface. [20] The formed intermediate ii stabilizes itself by reformation of the P-O double bond and opening of the five membered ring. This forms the intermediate iv bearing an alkoxide group, which can attack another phosphate molecule and thus propagate the polymer chain. However, instead of opening the five membered ring, the intermediate structure ii can also stabilize itself by eliminating the side chain as the alkoxide iii and thereby terminate the polymer chain. As this side reaction can take place for every added monomer, its likelihood will determine the overall effectiveness of the protective CEI film formation. Thus, the nature of the phospholane's side chain can be expected to be a very important factor in determining whether chain propagation or chain termination is favored over the other. For sterically demanding side chains, the side chain elimination reduces steric strain, thus making the cleavage of sterically demanding chains more favorable than the cleavage of sterically less demanding side chains. Another important influence is the stabilization of the charge of alkoxide iii. Electron withdrawing groups (EWGs) stabilize the negative charge, thus favoring its formation, while electron donating groups (EDGs) destabilize it and disfavor its formation.

Based on the latter considerations, one would expect the tert-butyl substituted additive tBuEPi to be the best performing one as it strongly disfavors the formation of the alkoxide species iii, thus disfavoring the cleavage reaction. The opposite is true for the fluorinated version, namely NFtBuEPi. Here, the strong EWGs should favor the formation of alkoxide iii while further favoring cleavage of the side chain, due to the even greater steric demand than in the non-fluorinated analogue. [21] These two functional additives should pretty clearly represent the edge cases, whereas it is rather difficult to estimate the effects of the intermediate structures.

Since phospholanes are well known to polymerize in the presence of Lewis acids, an alternative mechanism that does not rely on quantitative oxidation of the phospholane (Scheme 2) can be proposed. [22] In this case, the first step is the coordination of a phospholane molecule to a metal cation with the lone pair of phosphorus. The metal ion itself can be part of a surface (e.g. NMC111 cathode or lithium salt on the anode) or be solvated in the electrolyte. Another phospholane molecule can then attack the activated intermediate v nucleophilically. thus leading to ring opening and formation of intermediate vi. The chain propagates thereafter, through repeated nucleophilic attack, forming a surface bound polyphosphonate. If the side chain is susceptible to a nucleophilic attack, intermediates v and vi can undergo a chain transfer reaction instead of the ring opening.

Based on this mechanism, the most important factors can be expected to be the phospholane's nucleophilicity as well as the stabilization of intermediate vi as both influence the chain propagation step of the polymerization reaction.

Electron donating side chains increase the phospholane's nucleophilicity and stabilize intermediate vi, thus favoring the chain propagation reaction. However, an increasing steric demand of the side chain lowers the phospholane's nucleophilicity, which counteracts electron donating effects. From chemical intuition alone, it is difficult to estimate which effect dominates for each functional additive. However, as the stabilization of intermediate vi mostly depends on the sidechain's electron withdrawing or donating effect, it can be



Scheme 1. Postulated mechanism for the formation of polyphosphates from phospholanes on a NMC111 surface.

$$\begin{array}{c} \text{NMC} & \overset{\circ}{\underset{P}{\longrightarrow}} & \overset{\circ}{\underset{P}{\longrightarrow}}$$

Scheme 2. Postulated mechanism for the formation of polyphosphonates from phospholanes on a NMC111 surface.

expected that the intermediate's formation will take place most readily in case of tBuEPi due to its strongly electron donating side chain. The highly fluorinated functional additives can therefore be expected to disfavor the formation of intermediate vi and thus the overall polymerization reaction.

In order to shed more light on our considerations based on both the phosphate as well as the phosphonate mechanism, we performed DFT calculations of the key reaction steps for both suggested mechanisms. In particular, we performed calculations at the  $\omega B97XD/6-31+G(d,p)$  level of theory for the following reactions: To mimic the reactions from ii to iii (cleavage of side chain) or from ii to iv (ring opening) without the explicit NMC surface, which would be computationally significantly more expensive, [23,24] we focused on the analogous reactions of compound i to which methanolate has been added via a nucleophilic attack at the phosphorus atom of i in the calculations (see Scheme S1 in SI, note that similar results are obtained when replacing the activating methoxy group by a methoxy ethoxy group). For all reactions, we computed a) the change in the electronic energy (or reaction energy)  $\Delta E$ including a vibrational zero-point correction and b) the free energy difference (or reaction free energy)  $\Delta G$  including all thermal contributions. While the former quantity describes the potential energy surface of reactants and products and thus their relative energetic stability, the latter additionally accounts for thermodynamic (i.e. entropic and enthalpic) effects. The resulting values for the two reactions are shown in Figure 2. To probe the mechanism depicted in Scheme 2 (i.e. the phosphonate mechanism), we additionally calculated  $\Delta E$  and  $\Delta G$  for the reaction from v to vi. In this case, a methyl group was used to mimic the activation of intermediate  $\mathbf{v}$  (Scheme S1).

To evaluate the role of the depicted chain transfer reaction,  $\Delta E$  and  $\Delta G$  for the reaction from  ${\bf v}$  to  ${\bf vii}$  as well as the energy barriers for the aforementioned transformations were also calculated and are displayed in Figure 3. For both mechanisms, focus was set on the propagation or termination reaction of the polymerization rather than on the initial binding to the NMC surface, which would be computationally much more demanding (the presence of a phosphorous-containing CEI we can infer from previous XPS measurements). [16] To avoid superimposed conformational effects, same conformers of the reactant/

product/intermediate states displayed in in Schemes 1 and 2 were used for all different side groups.

For the phosphate mechanism the resulting reaction energies show a clear trend for the ring opening reaction (Figure 2a)): With decreasing fluorination degree, the resulting free energies drop to a plateau for the intermediate structures of TFnPrEPi, nPrEPi and iPrEPi, before dropping to almost 0 kcal·mol<sup>-1</sup> for tBuEPi. (slightly non-monotonous behavior between nPrEPi and iPrEPi can be attributed to marginal differences in the intramolecular interactions between the side group and the negatively charged alkoxide oxygen atom of the opened ring).

The opposite trend as in Figure 2a is observed for the cleavage reactions (Figure 2b)), for which the reaction (free) energy increases with decreasing fluorination degree. In particular, a clear transition from negative energy values for the highly fluorinated species to positive energy values for the less fluorinated species can be observed. Here, two partly opposing factors play a role (cf. our arguments in the introduction): First, the stabilization of the negatively charged alkoxide after cleavage of the side group by electron withdrawing effects, and second, the steric strain the side group exerts, with bulky groups favoring cleavage more than less bulky ones. For the electron withdrawing effect, one would expect increasing alkoxide stabilization in the order NFtBuEPi > HFiPrEPi > TFnPrE-Pi > nPrEPi > iPrEPi > tBuEPi, which is compatible with the trend of the fluorinated additives in Figure 2b, while for the nonfluorinated ones, the reverse trend is found (albeit weaker). The latter observation can be attributed to the increasing steric demand of iPrEPi and tBuEPi as compared to nPrEPi. Therefore, for the non-fluorinated additives, the steric effect overcompensates the electron withdrawing effect, whereas for the fluorinated ones, the steric effect (increasing as TFnPrEPi < HFiPrEPi < NFtBuEPi) enhances the electron withdrawing effect.

Calculations of the energy barriers reveal very similar magnitudes for all considered functional additives except for the highly fluorinated NFtBuEPi, amounting to  $\approx 10~\text{kcal} \cdot \text{mol}^{-1}$  in case of the ring opening reaction (Figure 2 c)). Significantly larger barrier for NFtBuEPi of as much as  $\approx 30~\text{kcal/mol}$  can be rationalized as follows: In all cases except NFtBuEPi, the transition states for the ring opening reaction are stabilized by



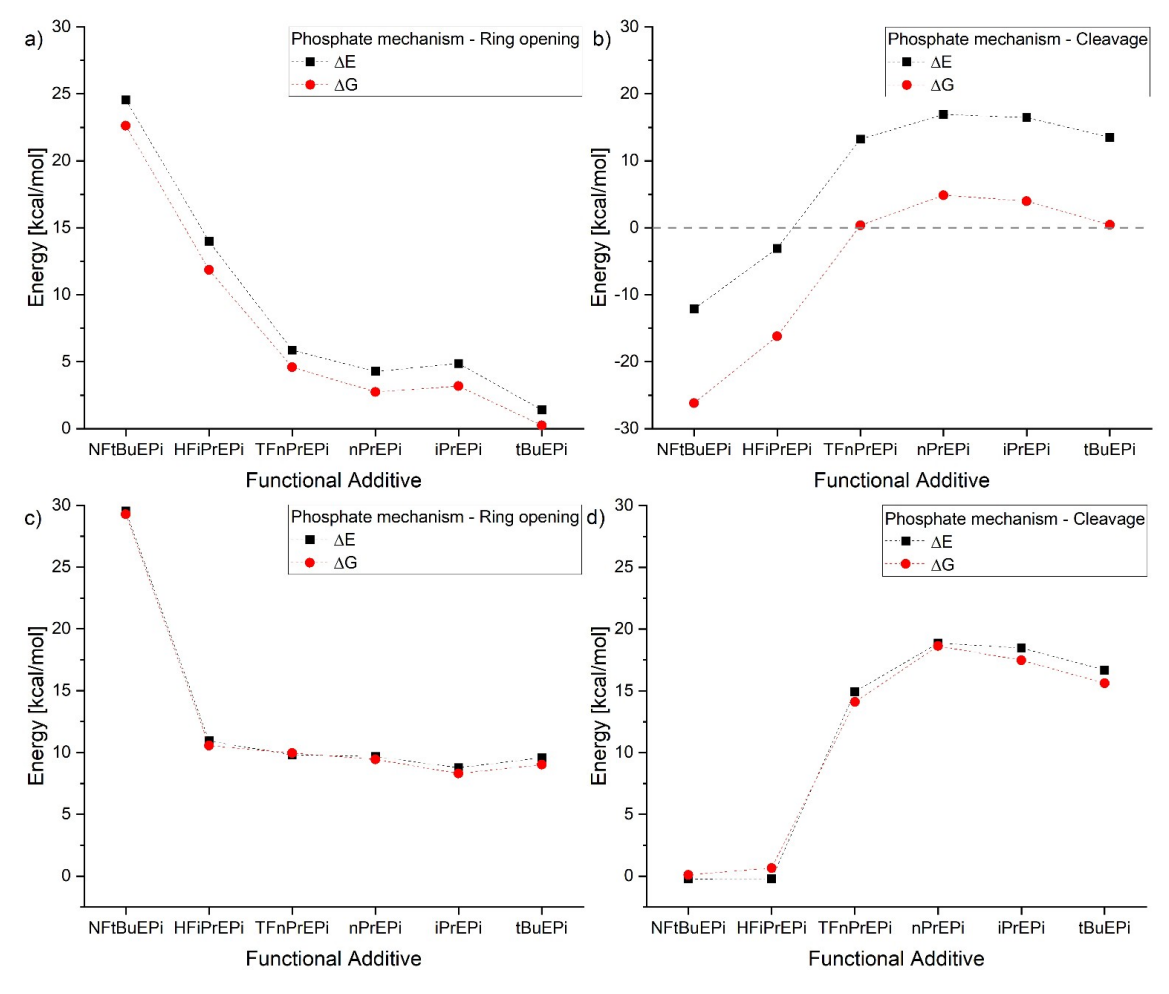


Figure 2. Calculated reaction energies  $\Delta E$ , reaction free energies  $\Delta G$  and energy barriers for the phosphate mechanism. a) Reaction energy of the ring opening reaction. b) Reaction energy of the cleavage reaction. c) Energy barrier of the ring opening reaction. d) Energy barrier of the cleavage reaction.

an intramolecular interaction between the alkoxide oxygen atom of the opening ring and an aliphatic proton from the  $\alpha\text{--}$ or  $\beta$ -carbon atom of the side chain. As the latter are missing in the fully fluorinated NFtBuEPi side group, no such stabilization is possible. Such interactions are likely formed with a molecule from the intermolecular environment in the electrolyte, which would result in an almost constant ring opening activation energy for all compounds.

Contrarily, in case of the cleavage reaction there is a clear distinction between the highly fluorinated additives NFtBuEPi and HFiPrEPi, that both feature barriers close to 0 kcal·mol<sup>-1</sup>, and the other structures, where the barriers lie well above 10 kcal·mol<sup>-1</sup>. As before, solvation effects might play a role under experimental solution conditions, which would lead to numerically different values. Nonetheless, we expect that the overall trend remains unaffected. Therefore, according to the scenario of the phosphate mechanism, highly fluorinated additive molecules tend to decompose via cleavage of the side chain, reflected by negative  $\Delta G$  values in Figure 2b) and largely positive  $\Delta G$  in Figure 2a) as well as very low energy barriers in Figure 2 d), while non-fluorinated species with electron-donating side groups may undergo the formation of iv (only slightly positive ring-opening energies in Figure 2a)),

although in the latter case the  $\Delta G$  values for the competing side-chain cleavage reaction are comparable in magnitude. However, as the energy barriers for the cleavage reaction are strongly positive (Figure 2 d)), the ring opening reaction is clearly favored in these cases.

Furthermore, even though the  $\Delta G$  values in Figure 2a) are slightly positive for the non-fluorinated species, one should keep in mind that this energy is compensated by an energy gain from the subsequent addition of another phosphate molecule. At the same time, the simultaneous presence of both mechanisms, even though with different relative occurrence, is compatible with the formation of a CEI with moderate thickness,[16] which is sufficiently thick to prevent continuous electrolyte oxidation but at the same time thin enough that it does not impede the overall cell performance due to large interfacial resistances, thus potentially giving rise to enhanced cvcle life.

In case of the phosphonate mechanism, the difference between the individual functional additives is less pronounced in the ring opening reaction. Although the calculated reaction



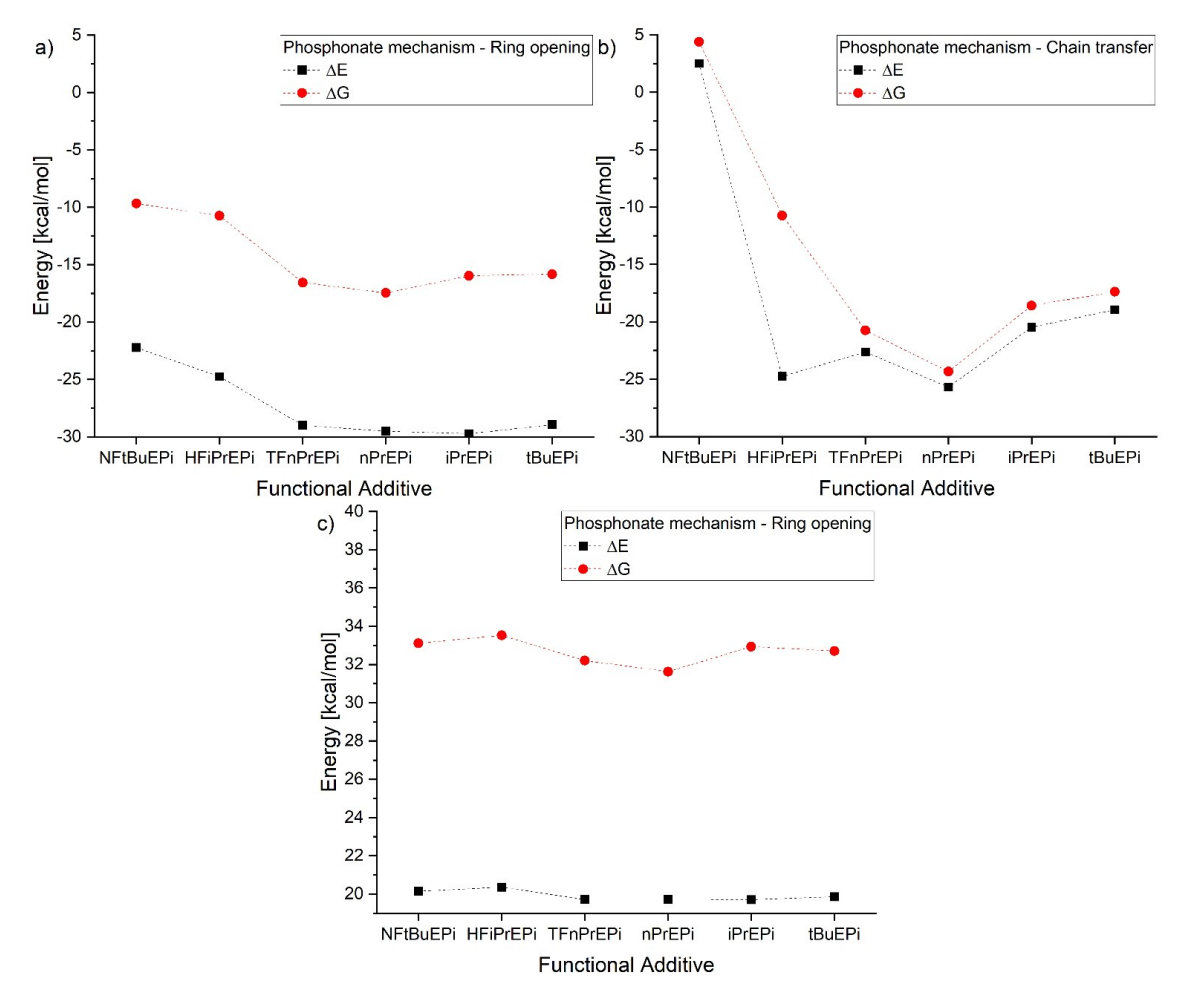


**Figure 3.** Calculated reaction energies  $\Delta E$ , free reaction energies  $\Delta G$  and energy barriers for the phosphonate mechanism. a) Reaction energy of the ring opening reaction. b) Reaction energy of the chain transfer reaction. c) Energy barrier of the ring opening reaction.

energies are strongly negative (Figure 3 a)), the energy barriers are strongly positive (Figure 3 c)) and exceed the ones found for the phosphate mechanism roughly by a factor of 2. In case of the competing chain transfer reaction, the reaction energies show mostly negative values of comparable magnitude as for the ring opening reaction (Figure 3 b)). Only in the case of the highly fluorinated NFtBuEPi positive values can be observed. From a computational point of view, both the phosphate mechanism as well as the phosphonate mechanism seem reasonable. However, the phosphate mechanism features much more accessible energy barriers as well as a much clearer distinction between the functional additives with strongly different chemical nature and thus seems to provide the overall better explanation.

Complementary experimental data were gained from galvanostatic cycling in NMC111||graphite CR2032 coin cells in a voltage range of 2.8–4.5 V (Figure 4). As a reference electrolyte (REF), a 1 M solution of LiPF $_6$  in a 1:1 mixture by weight of ethylene carbonate (EC) and ethyl methyl carbonate (EMC) was used. Additive containing electrolytes were gained by mixing in of 0.5 weight% of each functional additive to the reference electrolyte. It can be clearly seen, that the functional additives

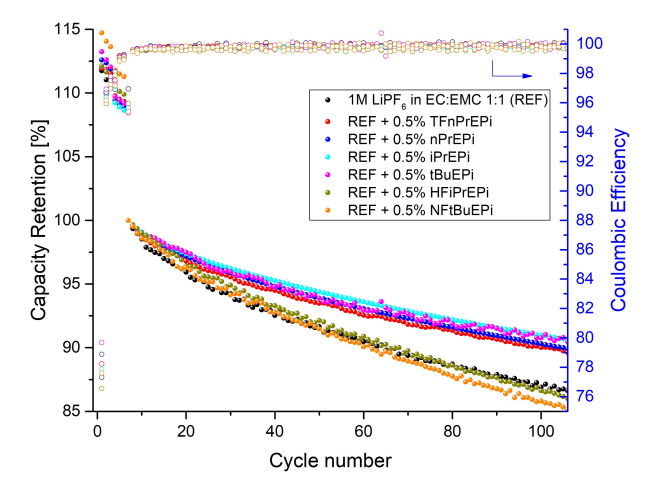


**Figure 4.** Capacity retention vs. cycle number curves of NMC111||graphite CR2032 cells containing the different additives cycled at 1 C in a voltage range of 2.8-4.5 V at  $20\,^{\circ}\text{C}$ .

with linear side chains as well as the non-fluorinated branched additives significantly improve the cycling performance compared to the reference electrolyte. While the differences in



cycling performance are only minor between these functional additives during the first 100 cycles, the sterically demanding non-fluorinated additives show a slight tendency towards better performance than the linear ones.

The strongly fluorinated additives even deteriorate the cycling performance compared to the reference electrolyte counterpart. As indicated by the DFT calculations, the branched, highly fluorinated additives HFiPrEPi and NFtBuEPi favor cleavage of the side chain over polymerization (Figure 2), thus liberating alkoxide species that can potentially interfere with film formation on both electrodes and deteriorate the overall performance. It has been shown that methoxide and ethoxide species have a detrimental effect on CEI formation on NMC111 material and thus on the overall cycling performance. [25,26] It is therefore safe to assume, that other alkoxide species will have similar effects.

When the calculated energy values are plotted against the achieved capacity retention after 100 charge/discharge cycles for each functional additive, a strong correlation becomes obvious (Figure 5 a), b)). The overall cell performance is positively correlated to the calculated reaction energy of the cleavage reaction and negatively correlated to the energy of the ring opening reaction. Furthermore, a similar positive correlation is found for the calculated energy barrier of the cleavage reaction (Figure 5 c)) while the energy barrier of the ring opening reactions seems to be only loosely correlated to the capacity retention (here, the NFtBuEPi transition state constitutes an outlier due to the absence of a stabilizing hydrogen bond, see above).

In case of the phosphonate mechanism, there is an apparently linear correlation of the calculated energy values of the ring opening reaction with the capacity retention after 100 cycles as well (Figure 6 a) and b)), albeit with a much smaller magnitude than in the previous case. In case of the chain transfer reaction, the findings are inconclusive as the values show a large variability on the energy axis. The calculated energy barriers for the ring opening reaction are clearly noncorrelated to the capacity retention as their values are almost identical for all considered additive structures (Figure 6 c) and d)). These findings confirm the considerations previously made for the suggested phosphate mechanism. In fact, the possibility of clearly correlating such a complex observable as the overall cycling performance, reflected in the capacity retention, to the calculated energy values and energy barriers strongly suggests that the proposed mechanism is indeed the mode of action of phospholane additives in lithium ion batteries. Therefore, our

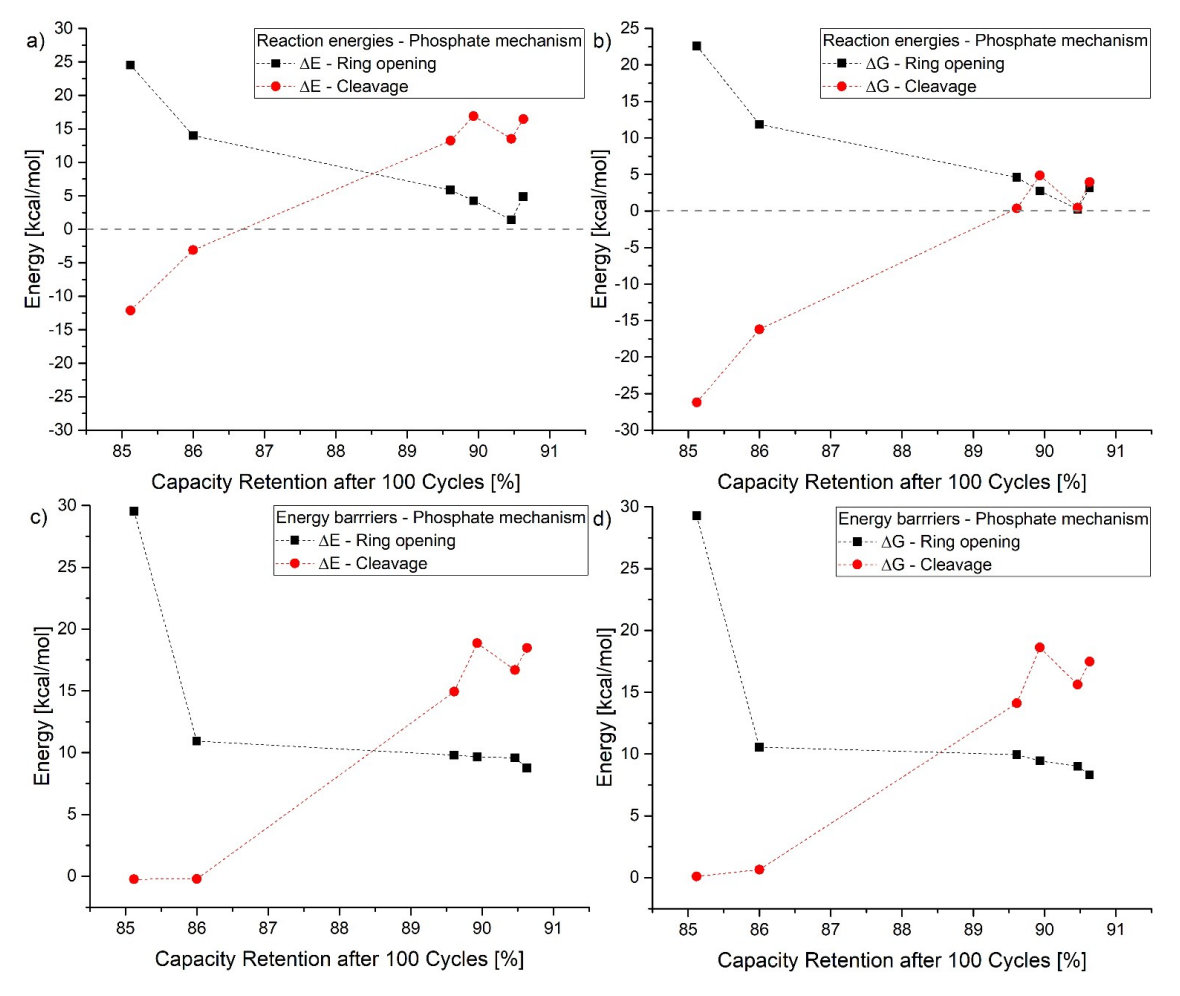


Figure 5. Calculated reaction energies and energy barriers vs. capacity retention after 100 cycles for the phosphate mechanism. a, c) Calculated reaction energies  $\Delta E$  and b, d) free reaction energies  $\Delta G$ .

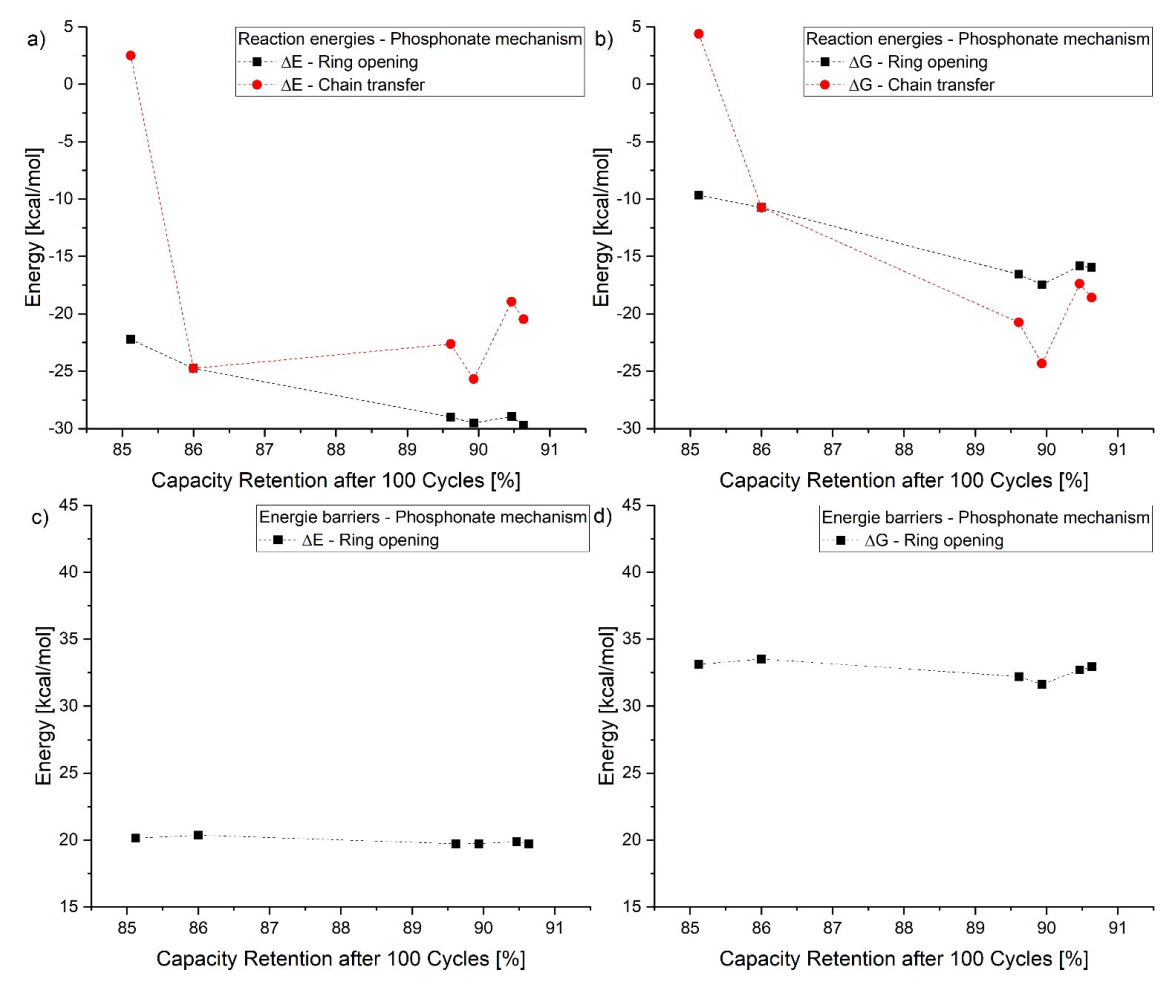
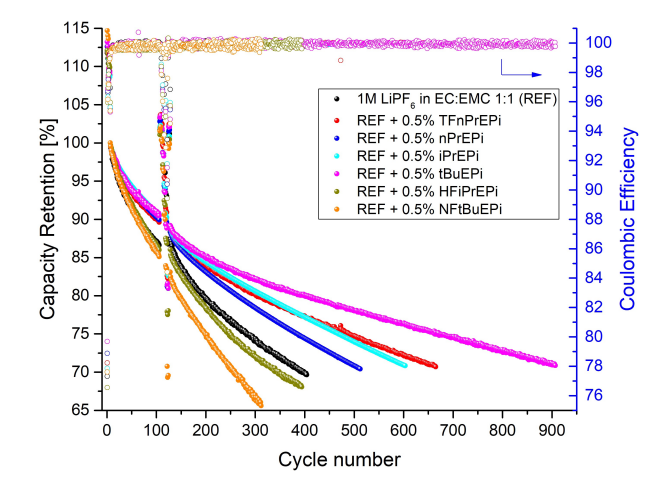


Figure 6. Calculated reaction energies and energy barriers vs. capacity retention after 100 cycles for the phosphonate mechanism. a,c) Calculated reaction energies ΔE and b,d) free reaction energies ΔG.

findings are also encouraging for large-scale computational screening approaches for this class of functional additives.<sup>[27–30]</sup>

The phosphonate mechanism can be ruled out as there is no clear correlation of the calculated energy values and energy barriers with the observed cycling performance. Furthermore, we speculate that compound **iv** of the phosphate mechanism could in principle initiate copolymerization with EC,<sup>[31,32]</sup> which is more abundant in the electrolyte than the functional additive itself. In such a scenario, quantitative oxidation of the functional additive (reaction to **i**) would not be required, thus also clearly supporting the phosphate mechanism.

After 100 cycles, the NMC111||graphite cells were subjected to a C-rate test and a subsequent galvanostatic cycling at 1 C until reaching the end of life (EOL) criterion (dropped to 80% of the capacity after the C-rate test) (Figure 7). While the previously observed trends remain mostly the same, individual cells with the same electrolyte formulation tend to diverge from each other towards their EOL as small differences accumulate over the long period of galvanostatic cycling. Therefore, it is rather difficult to predict a cell's exact EOL from the first 100 cycles. However, the long-term cycling data confirm the previous conclusion that, based on the phosphate mechanism,



**Figure 7.** Long-term cycling performance of NMC111||graphite CR2032 cells containing different functional electrolyte additives at 1 C in the voltage range of 2.8- 4.5 V and at 20 °C under EOL criterion (80% of the discharge capacity of cycle 130 (after the C-rate test) is reached).



among the considered functional additives the non-fluorinated tBuEPi should perform best, whereas the fluorinated NFtBuEPi should show the poorest performance.

The reason for the tremendous difference in cycling performance becomes evident from SEM micrographs taken after the NMC111||graphite cells reached their respective EOL criterion. In case of the reference electrolyte as well as the electrolyte containing the perfluorinated NFtBuEPi, the negative electrode's graphite particles are completely covered in a thick surface layer (Figure 8 b) and c)). The surface film appears to be smoothing out the graphite's surface features more effectively in case of NFtBuEPi, which may be an indication of a larger surface layer thickness. Furthermore, there are small granular particles on the surface, giving it a grainy appearance. In case of the non-fluorinated tBuEPi, the graphite particles have a distinctively different appearance. While a dense surface layer is also present in this case, the graphite primary particle's features are smoothed out much less than in the cases discussed before.

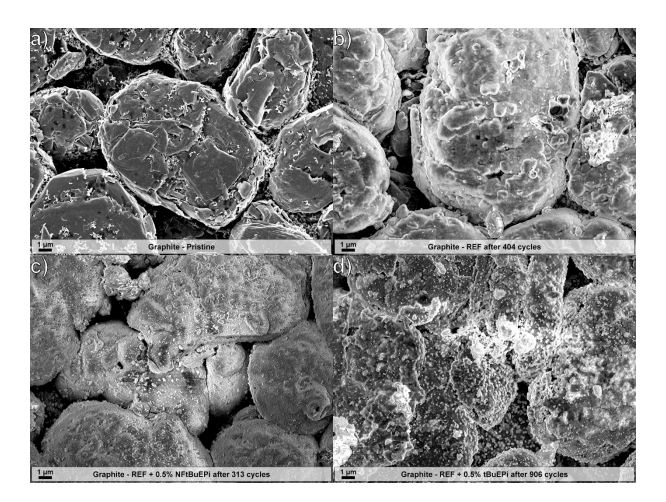


Figure 8. SEM images of graphite negative electrodes: a) pristine, b) with REF after 404 cycles, c) with REF + NFtBuEPi after 313 cycles, d) with REF + tBuEPi after 906 cycles.

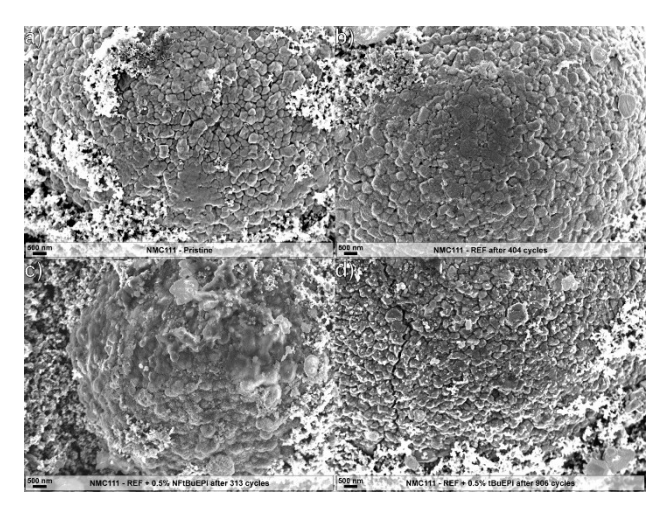


Figure 9. SEM images of NMC111 positive electrodes: a) pristine, b) with REF after 404 cycles, c) with REF + NFtBuEPi after 313 cycles, d) with REF + tBuEPi after 906 cycles.

Furthermore, it features a homogeneous covering in small globular particles, which is not observed in the other cases (Figure 8 d). This clearly indicates that while designed to be effective on the positive electrode, phospholane functional additives significantly alter the solid electrolyte interphase (SEI)[33] chemistry.

In case of the reference electrolyte, a surface layer is formed on the positive electrode, which gives the NMC111 primary particles a rougher appearance compared to the pristine material (Figure 9 a) and b)). However, the layer must be much thinner than on the negative electrode, since the primary particles can still be clearly seen. The non-fluorinated tBuEPi forms a smoother surface layer with an additional light coverage of globular particles that resemble the ones observed on the negative electrode, but are smaller in size (Figure 9 d)). The perfluorinated NFtBuEPi on the other hand leads to the formation of a very thick surface layer, that covers the complete NMC111 secondary particles (Figure 9 c)). This surface layer is clearly the reason for the poor performance even compared to the reference electrolyte. A recent study revealed impedance growth on the positive electrode and especially transition metal dissolution from its active material to be the predominant reasons for capacity fading and in some cases even rapid cell failure, known as "rollover" failure, in NMC532||graphite cells under high voltage conditions. [34] In line with this, the formation of an effective CEI by the studied phospholane functional additives evidently alters these processes and is thus beneficial for an enhanced battery performance.

In conclusion, on a qualitative level, the SEM micrographs clearly show that phospholanes alter the CEI as originally proposed with the phosphate mechanism.[16] However, it is evident that they furthermore have a significant influence on the SEI as well.

### 3. Conclusions

We designed and synthesized six phospholane functional molecules that feature small, incremental changes to their steric and electronic properties in order to understand their mode of action as film-forming (CEI) additives in lithium ion battery electrolytes. To do so, we proposed two mechanisms and conducted a DFT study of the key reaction steps as well as their side reactions for both mechanisms. The DFT results can be strongly correlated to the galvanostatic cycling performance of NMC111||graphite cells with functional additive containing electrolyte under high voltage conditions. We thus conclude that phospholane additives do indeed polymerize on NMC111 surface via proposed phosphate mechanism. The possibility of directly correlating a complex observable as the cycling performance to structural features of the used electrolyte chemistry, that is directly accessible by DFT calculations, is very encouraging and promises to be an approach for future theory supported tailored synthesis and screening endeavors.



# **Experimental Section**

### **Electrolyte and Cell Preparation**

A 1 M solution of LiPF<sub>6</sub> in ethylene carbonate (EC) and ethyl methyl carbonate (EMC) (1:1 by weight) was used as the reference electrolyte (REF). Electrolytes containing additives were made by addition of 0.5 wt% of appropriate additive to the reference electrolyte. Additive containing electrolytes were freshly prepared prior to cell assembly. Graphite and NMC111 electrodes were purchased from *Customcells*°. One layer of *Separion*° was used as a separator. Electrodes and separators were dried at 120 °C under vacuum for 16 h prior to use. CR2032 type two-electrode<sup>[35]</sup> coin cells were assembled in the dry room (dew point < -60°C).

### **Electrochemical Characterization**

Galvanostatic cycling was performed on a battery tester (MACCOR series 4000) in the voltage range of 2.8 V to 4.5 V. Formation was done by cycling the cells at C/10 and C/3 for three cycles each. After formation, cells were cycled at 1 C for 100 charge/discharge cycles, followed by a C-rate test, and thereafter cycling at 1 C until reaching 80% of the cell capacity (after the C-rate test).

#### Post Mortem Analysis via SEM

For scanning electron microscopy (SEM) the electrodes were washed with dimethyl carbonate (1 mL) and analyzed using an *Auriga® CrossBeam workstation (Zeiss)* at an acceleration voltage of 3 kV at a working distance of 3 mm using the InLens detector.

### **Quantum Chemical Calculations**

All calculations were performed with the Gaussian 16 package. [36] We chose the range-separated exchange-correlation functional ωB97XD<sup>[37]</sup> including empirical dispersion<sup>[38]</sup> in combination with the 6–31 + G(d,p) basis set. [39–41] The implicit SMD solvent model [42] was used with built-in solvent parameters for acetone in all calculations, mimicking the relative permittivity of typical carbonate solvents.  $^{\left[ 29,43,44\right] }$  For the individual reaction steps (Scheme S1) for different side groups (Figure 1), care was taken that the conformations of the phospholane moiety of all compounds were identical. To assess the effect of the basis set on the results, additional single point calculations were carried out with the 6-311+G(d,p) basis set  $^{[45,46]}$  with thermochemical information derived at the  $\omega B97XD/6\text{-}$ 31 + G(d,p) level of theory (see Supporting Information). We find an overall mean absolute deviation (MAD) of 0.58 kcal·mol<sup>-1</sup> when comparing both basis sets (precisely, MAD=0.75 kcalmol<sup>-1</sup> for the ring opening reactions and MAD=0.30 kcal·mol<sup>-1</sup> for the cleavage reactions according to the phosphate mechanism as well as MAD= 1.0 kcal·mol<sup>-1</sup> for the ring opening reactions and MAD= 0.28 kcal·mol<sup>-1</sup> for the chain transfer reactions according to the phosphonate mechanism). Since we do not aim to reproduce the reaction energies with chemical accuracy, but rather to correlate their trends to the experimental data, the above results demonstrate that the computationally more expedient 6-31+G(d,p) basis set is sufficiently accurate for our purpose.

### **Synthesis**

All considered functional additives were synthesized in flame-dried glassware under an atmosphere of argon using standard Schlenk-techniques.  $Et_2O$  and THF were dried using a *PureSolv* solvent purification system (*Inert Corporation*). 2-Propanol and pyridine

were dried over Na and distilled and stored over 3 Å molecular sieves under Ar prior to use. PCI<sub>3</sub> was distilled and stored under Ar prior to use.

# Synthesis of 2-(3,3,3-Trifluoropropoxy)-1,3,2-dioxaphospholane (TFnPrEPi)

PCl<sub>3</sub> (3.8 mL, 43.44 mmol) and pyridine (10.5 mL, 130.35 mmol) were dissolved in dry Et<sub>2</sub>O (300 mL) and the solution cooled to 0 °C. Then ethylene glycol (2.5 mL, 44.71 mmol) was added dropwise over a period of 10 min. The formed suspension was stirred for 10 min at room temperature and cooled to 0 °C again. Thereafter, 3,3,3-trifluoropropan-1-ol (5.025 g, 44.05 mmol) was added dropwise over a period of 5 min, leading to formation of more precipitate. After stirring at room temperature overnight, the solid was separated by cannula filtration and NaH (0.44 g; 60 % slurry in paraffin) was added to the supernatant solution. The suspension was stirred for 20 min at room temperature and the solvent removed with a condensation trap at room temperature under a pressure of 40 mbar. Fractioned distillation of the residue through a Vigreux column yielded the product (2.660 g, 30 %; 80 °C, 40 mbar) as a colorless liquid. <sup>1</sup>H NMR (400 MHz, 300 K, CDCl<sub>3</sub>):  $\delta$  = 4.19 (m, 2H, OCH<sub>2</sub>), 4.00 (m, 4H, OCH<sub>2</sub>), 2.40 (qt,  ${}^{3}J_{FH} = 10.5$  Hz,  ${}^{3}J_{HH} = 6.6$  Hz, 2H, CH<sub>2</sub>CF<sub>3</sub>). <sup>19</sup>**F NMR** (376 MHz, 300 K, CDCl<sub>3</sub>):  $\delta = -64.83$  (td,  ${}^{3}J_{FH} =$ 10.5 Hz,  ${}^5J_{PF} = 1.8$  Hz).  ${}^{31}P\{{}^1H\}$  NMR (162 MHz, 300 K, CDCl<sub>3</sub>):  $\delta =$ 134.98 (q,  ${}^{5}J_{PF} = 1.8 \text{ Hz}$ ).

### Synthesis of 2-Propoxy-1,3,2-dioxaphospholane (nPrEPi)

2-Chloro-1,3,2-dioxaphospholane (6.0 mL, 67.46 mmol) and pyridine (5.4 mL, 67.04 mmol) were dissolved in dry Et<sub>2</sub>O (50 mL) and the solution cooled to 0 °C. Thereafter 1-propanol (5.0 mL, 67.29 mmol) was added dropwise over a period of 5 min, leading to the formation of a colorless precipitate. The suspension was allowed to warm to room temperature and stirred overnight. After filtering through a plug of Celite and rinsing with Et<sub>2</sub>O (100 mL), the solvent was removed with a condensation trap at room temperature under a pressure of 40 mbar. Fractioned distillation of the residue through a Vigreux column yielded the product (2.930 g, 28%; 81°C, 40 mbar) as a colorless liquid. <sup>1</sup>H NMR (400 MHz, 300 K,  $C_6D_6$ ):  $\delta$  = 3.68 (m, 2H,  $OCH_2^{P_1}$ ), 3.50 (m, 2H,  $OCH_2CH_2O$ ), 3.37 (m, 2H,  $OCH_2CH_2O$ ), 1.38 (m, 2H,  $CH_2^{P_1}$ ), 0.75 (t,  $^3J_{HH}$  = 7.4 Hz, 3H,  $CH_3$ ). <sup>31</sup>P  $\{^1H\}$  NMR (162 MHz, 300 K,  $C_6D_6$ ):  $\delta$  = 135.25.

### Synthesis of 2-Isopropoxy-1,3,2-dioxaphospholane (iPrEPi)

2-Chloro-1,3,2-dioxaphospholane (6.0 mL, 67.46 mmol) and pyridine (5.4 mL, 67.04 mmol) were dissolved in dry Et<sub>2</sub>O (200 mL) and the solution cooled to 0 °C. 2-Propanol (5.2 mL, 67.49 mmol) was added dropwise over a period of 5 min, leading to the formation of a colorless precipitate. The suspension was allowed to warm to room temperature and stirred overnight. After filtering through a plug of Celite, the solvent was removed with a condensation trap at room temperature under a pressure of 40 mbar. Fractioned distillation of the residue through a Vigreux column yielded the product (3.588 g, 35 %; 39 °C, 10 mbar) as a colorless liquid.  $^1\text{H}$  NMR (400 MHz, 300 K,  $C_6D_6$ ):  $\delta$  = 4.14 (dhept,  $^3J_{\text{PH}}$  = 8.8 Hz,  $^3J_{\text{HH}}$  = 6.2 Hz, 1H, CHiP), 3.71 (m, 2H, OCH<sub>2</sub>CH<sub>2</sub>O), 3.38 (m, 2H, OCH<sub>2</sub>CH<sub>2</sub>O), 1.04 (d,  $^3J_{\text{HH}}$  = 6.2 Hz, 6H, CH<sub>3</sub>IP).  $^3\text{Pf}^1\text{H}$  NMR (162 MHz, 300 K,  $C_6D_6$ ):  $\delta$  = 135.84.

### Synthesis of 2-tert-Butoxy-1,3,2-dioxaphospholane (tBuEPi)

2-Chloro-1,3,2-dioxaphospholane (6.0 mL, 67.46 mmol) and pyridine (5.5 mL, 68.28 mmol) were dissolved in dry  $\rm Et_2O$  (200 mL) and the



solution cooled to 0°C. A solution of tert-butanol (6.4 mL, 68.21 mmol) in dry Et<sub>2</sub>O (50 mL) was added dropwise over a period of 10 min, forming a colorless precipitate. The suspension was allowed to warm to room temperature and stirred overnight. After filtering through a plug of Celite, the solvent was removed with a condensation trap at room temperature under a pressure of 40 mbar. Fractioned distillation of the residue through a Vigreux column yielded the product (3.039 g, 27%; 74°C, 40 mbar) as a colorless liquid.  $^{1}H$  NMR (400 MHz, 300 K,  $C_{6}D_{6}$ ):  $\delta = 3.79$  (m, 2H, OCH<sub>2</sub>CH<sub>2</sub>O), 3.40 (m, 2H, OCH<sub>2</sub>CH<sub>2</sub>O), 1.26 (s, 9H, <sup>t</sup>Bu). <sup>31</sup>P{<sup>1</sup>H} NMR (162 MHz, 300 K,  $C_6D_6$ ):  $\delta = 134.77$ .

## Synthesis of 2-(1,1,1,3,3,3-Hexafluoroisopropoxy)-1,3,2-dioxaphospholane (HFiPrEPi)

2-Chloro-1,3,2-dioxaphospholane (6.0 mL, 67.46 mmol) and pyridine (5.4 mL, 67.04 mmol) were dissolved in dry Et<sub>2</sub>O (200 mL) and the solution cooled to 0°C. Thereafter, 1,1,1,3,3,3-hexafluoroisopropanol (7.2 mL, 68.38 mmol) was added dropwise over a period of 10 min, leading to the formation of a colorless precipitate. The suspension was allowed to warm to room temperature and stirred overnight. After filtering through a plug of Celite, the solvent was removed with a condensation trap at room temperature under a pressure of 80 mbar. Fractioned distillation of the residue through a Vigreux column yielded the product (11.068 g, 63 %; 42 °C, 20 mbar) as a colorless liquid. <sup>1</sup>H NMR (400 MHz, 300 K,  $C_6D_6$ ):  $\delta = 4.01$  (dhept,  $^{3}J_{PH} = 8.1 \text{ Hz}, ^{3}J_{FH} = 5.9 \text{ Hz}, 1H, CF_{3}CH), 3.46 (m, 2H, OCH_{2}CH_{2}O), 3.11$ (m, 2H, OCH<sub>2</sub>CH<sub>2</sub>O). <sup>19</sup>**F**{<sup>1</sup>**H**} **NMR** (376 MHz, 300 K, C<sub>6</sub>D<sub>6</sub>):  $\delta$ =-74.58 (d,  ${}^4J_{PF} = 7.3 \text{ Hz}$ ).  ${}^{31}P\{{}^1H\}$  NMR (162 MHz, 300 K,  $C_6D_6$ ):  $\delta = 140.35$ (hept,  ${}^{4}J_{PF} = 7.3 \text{ Hz}$ ).

# Synthesis of 2-Nonafluoro-tert-butoxy-1,3,2-dioxaphospholane (NFtBuEPi)

Nonafluoro-tert-butanol (1.645 g, 6.97 mmol) was dissolved in dry THF (50 mL) and the solution cooled to -70 °C. After dropwise addition of *n*-butyllithium (2.8 mL, 6.25 mmol; 2.5 M in hexanes), the solution was stirred for 10 min at -70 °C and allowed to warm to room temperature. It was cooled to 0°C again and 2-chloro-1,3,2dioxaphospholane (0.866 g, 6.85 mmol) was added, leading to the formation of a colorless precipitate. After addition of hexane (100 mL) and filtering through Celite, the solvent was removed with a condensation trap at room temperature under a pressure of 100 mbar. Fractioned distillation of the residue through a Vigreux column yielded the product (0.215 g, 9%; 27  $^{\circ}\text{C},$  10 mbar) as a colorless liquid. <sup>1</sup>H NMR (400 MHz, 300 K,  $C_6D_6$ ):  $\delta = 3.48$  (s, 2H, OCH<sub>2</sub>CH<sub>2</sub>O), 3.08 (m, 2H, OCH<sub>2</sub>CH<sub>2</sub>O). <sup>19</sup>F NMR (376 MHz, 300 K,  $C_6D_6$ ):  $\delta = -71.72$  (d, 25.1 Hz). <sup>31</sup>P{<sup>1</sup>H} NMR (162 MHz, 300 K,  $C_6D_6$ ):  $\delta = 134.76$  (m).

# **Acknowledgements**

This project has received funding from the European Union's Horizon 2020 research and innovation programme under grant agreement No 875548. Open access funding enabled and organized by Projekt DEAL.

# Conflict of Interest

The authors declare no conflict of interest.

Keywords: density functional calculations · electrochemistry · lithium-ion batteries · functional electrolyte additive · reaction mechanism

- [1] M. Li, J. Lu, Z. Chen, K. Amine, Adv. Mater. 2018, 30, 1800561.
- [2] R. Schmuch, R. Wagner, G. Hörpel, T. Placke, M. Winter, Nat. Energy **2018**, 3, 267-278.
- [3] M. Winter, R. J. Brodd, Chem. Rev. 2004, 104, 4245-4270.
- [4] S. Dühnen, J. Betz, M. Kolek, R. Schmuch, M. Winter, T. Placke, Small Methods 2020, 4, 2000039.
- [5] H. Zhang, H. Zhao, M. A. Khan, W. Zou, J. Xu, L. Zhang, J. Zhang, J. Mater. Chem. A 2018, 6, 20564-20620.
- [6] T. Placke, R. Kloepsch, S. Dühnen, M. Winter, J. Solid State Electrochem. 2017, 21, 1939-1964.
- [7] F. Duffner, R. Schmuch, J. Tübke, J. Leker, M. Winter, Nat. Energy n.d., in
- [8] J. B. Goodenough, Y. Kim, J. Power Sources 2011, 196, 6688-6694.
- [9] X. Zuo, C. Fan, X. Xiao, J. Liu, J. Nan, J. Power Sources 2012, 219, 94-99.
- [10] M. Winter, Z. Für Phys. Chem. 2009, 223, 1395-1406.
- [11] S. S. Zhang, J. Power Sources 2006, 162, 1379–1394.
- [12] K. Xu, Chem. Rev. 2014, 114, 11503-11618.
- [13] A. M. Haregewoin, A. S. Wotango, B.-J. Hwang, Energy Environ. Sci. 2016, 9, 1955-1988.
- [14] I. Cekic-Laskovic, N. von Aspern, L. Imholt, S. Kaymaksiz, K. Oldiges, B. R. Rad, M. Winter, Top. Curr. Chem. 2017, 375, 37.
- [15] C.-C. Su, M. He, C. Peebles, L. Zeng, A. Tornheim, C. Liao, L. Zhang, J. Wang, Y. Wang, Z. Zhang, ACS Appl. Mater. Interfaces 2017, 9, 30686-
- [16] N. von Aspern, D. Diddens, T. Kobayashi, M. Börner, O. Stubbmann-Kazakova, V. Kozel, G.-V. Röschenthaler, J. Smiatek, M. Winter, I. Cekic-Laskovic, ACS Appl. Mater. Interfaces 2019, 11, 16605-16618.
- [17] D. R. Gallus, R. Wagner, S. Wiemers-Meyer, M. Winter, I. Cekic-Laskovic, Electrochim. Acta 2015, 184, 410-416.
- [18] K. Kaluzynski, J. Libisowski, S. Penczek, Macromolecules 1976, 9, 365-367.
- [19] D. J. Lee, D. Im, Y.-G. Ryu, S. Lee, J. Yoon, J. Lee, W. Choi, I. Jung, S. Lee, S.-G. Doo, J. Power Sources 2013, 243, 831-835.
- [20] M. He, C.-C. Su, C. Peebles, Z. Feng, J. G. Connell, C. Liao, Y. Wang, I. A. Shkrob, Z. Zhang, ACS Appl. Mater. Interfaces 2016, 8, 11450-11458.
- [21] C. A. Tolman, Chem. Rev. 1977, 77, 313-348.
- [22] Y. Kawakami, K. Miyata, Y. Yuya, Polym. J. 1979, 11, 175-183.
- [23] O. Borodin, Curr. Opin. Electrochem. 2019, 13, 86-93.
- [24] N. von Aspern, M. Grünebaum, D. Diddens, T. Pollard, C. Wölke, O. Borodin, M. Winter, I. Cekic-Laskovic, J. Power Sources 2020, 461, 228159.
- [25] H.-J. Peng, S. Urbonaite, C. Villevieille, H. Wolf, K. Leitner, P. Novák, J. Electrochem. Soc. 2015, 162, A7072-A7077.
- [26] H.-J. Peng, C. Villevieille, S. Trabesinger, H. Wolf, K. Leitner, P. Novák, J. Power Sources 2016, 335, 91-97.
- [27] M. Korth, Phys. Chem. Chem. Phys. 2014, 16, 7919-7926.
- [28] T. Husch, M. Korth, Phys. Chem. Chem. Phys. 2015, 17, 22799-22808.
- [29] O. Borodin, M. Olguin, C. E. Spear, K. W. Leiter, J. Knap, Nanotechnology **2015**, 26, 354003.
- [30] L. Cheng, R. S. Assary, X. Qu, A. Jain, S. P. Ong, N. N. Rajput, K. Persson, L. A. Curtiss, J. Phys. Chem. Lett. 2015, 6, 283-291.
- [31] W. J. Evans, H. Katsumata, Macromolecules 1994, 27, 4011-4013.
- [32] J.-C. Lee, M. H. Litt, Macromolecules 2000, 33, 1618-1627.
- [33] P. Niehoff, S. Passerini, M. Winter, Lanamuir 2013, 29, 5806-5816.
- [34] S. Klein, P. Bärmann, T. Beuse, K. Borzutzki, J. E. Frerichs, J. Kasnatscheew, M. Winter, T. Placke, ChemSusChem 2020, DOI: 10.1002/ cssc.202002113.
- [35] R. Nölle, K. Beltrop, F. Holtstiege, J. Kasnatscheew, T. Placke, M. Winter, Mater. Today 2020, 32, 131-146.
- [36] M. J. Frisch, G. W. Trucks, H. B. Schlegel, G. E. Scuseria, M. A. Robb, J. R. Cheeseman, G. Scalmani, V. Barone, G. A. Petersson, H. Nakatsuji, X. Li, M. Caricato, A. V. Marenich, J. Bloino, B. G. Janesko, R. Gomperts, B. Mennucci, H. P. Hratchian, J. V. Ortiz, A. F. Izmaylov, J. L. Sonnenberg, D. Williams-Young, F. Ding, F. Lipparini, F. Egidi, J. Goings, B. Peng, A. Petrone, T. Henderson, D. Ranasinghe, V. G. Zakrzewski, J. Gao, N. Rega, G. Zheng, W. Liang, M. Hada, M. Ehara, K. Toyota, R. Fukuda, J. Hasegawa, M. Ishida, T. Nakajima, Y. Honda, O. Kitao, H. Nakai, T. Vreven, K. Throssell, J. A. Montgomery Jr, J. E. Peralta, F. Ogliaro, M. J. Bearpark, J. J. Heyd, E. N. Brothers, K. N. Kudin, V. N. Staroverov, T. A. Keith, R.

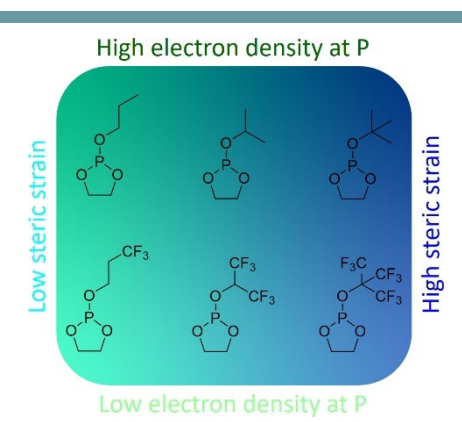


- Kobayashi, J. Normand, K. Raghavachari, A. P. Rendell, J. C. Burant, S. S. Iyengar, J. Tomasi, M. Cossi, J. M. Millam, M. Klene, C. Adamo, R. Cammi, J. W. Ochterski, R. L. Martin, K. Morokuma, O. Farkas, J. B. Foresman, D. J. Fox, *Gaussian 16 Rev. B.01*, Wallingford, CT, **2016**.
- [37] J.-D. Chai, M. Head-Gordon, Phys. Chem. Chem. Phys. 2008, 10, 6615–6620.
- [38] S. Grimme, J. Comput. Chem. 2006, 27, 1787-1799.
- [39] W. J. Hehre, R. Ditchfield, J. A. Pople, J. Chem. Phys. 1972, 56, 2257–2261.
- [40] M. M. Francl, W. J. Pietro, W. J. Hehre, J. S. Binkley, M. S. Gordon, D. J. DeFrees, J. A. Pople, J. Chem. Phys. 1982, 77, 3654–3665.
- [41] T. Clark, J. Chandrasekhar, G. W. Spitznagel, P. V. R. Schleyer, J. Comput. Chem. 1983, 4, 294–301.
- [42] A. V. Marenich, C. J. Cramer, D. G. Truhlar, J. Phys. Chem. B 2009, 113, 6378–6396.
- [43] O. Borodin, W. Behl, T. R. Jow, J. Phys. Chem. C 2013, 117, 8661-8682.
- [44] D. S. Hall, J. Self, J. R. Dahn, J. Phys. Chem. C 2015, 119, 22322–22330.
- [45] A. D. McLean, G. S. Chandler, J. Chem. Phys. 1980, 72, 5639-5648.
- [46] R. Krishnan, J. S. Binkley, R. Seeger, J. A. Pople, J. Chem. Phys. 1980, 72, 650–654.

Manuscript received: January 22, 2021 Revised manuscript received: February 18, 2021

# **ARTICLES**

Small change, big influence: Six phospholane electrolyte additives, featuring incremental changes to their structure, are synthesized for the first time and analyzed via complementary experimental and computational methods to understand their performance in NMC111||graphite battery cells under high voltage conditions. The computational results could be directly correlated to the overall cycling performance, resulting in elucidation and proposition of a reaction mechanism.



Dr. C. Wölke, Dr. D. Diddens, B. Heidrich, Prof. Dr. M. Winter, Dr. I. Cekic-Laskovic\*

1 - 12

Understanding the Effectiveness of Phospholane Electrolyte Additives in Lithium-Ion Batteries under High-Voltage Conditions





Understanding the Effectiveness of Phospholane #Electrolyte Additives in Lithium-Ion #Batteries under High-Voltage Conditions (Cekic-Laskovic & co-workers @fzj\_iek @WWU\_Muenster) #OpenAccess #ProjektDEAL

Share your work on social media! *ChemElectroChem* has added Twitter as a means to promote your article. Twitter is an online microblogging service that enables its users to send and read short messages and media, known as tweets. Please check the pre-written tweet in the galley proofs for accuracy. If you, your team, or institution have a Twitter account, please include its handle @username. Please use hashtags only for the most important keywords, such as #catalysis, #nanoparticles, or #proteindesign. The ToC picture and a link to your article will be added automatically, so the **tweet text must not exceed 250 characters**. This tweet will be posted on the journal's Twitter account (follow us @ChemElectroChem) upon publication of your article in its final (possibly unpaginated) form. We recommend you to re-tweet it to alert more researchers about your publication, or to point it out to your institution's social media team.

### **ORCID** (Open Researcher and Contributor ID)

Please check that the ORCID identifiers listed below are correct. We encourage all authors to provide an ORCID identifier for each coauthor. ORCID is a registry that provides researchers with a unique digital identifier. Some funding agencies recommend or even require the inclusion of ORCID IDs in all published articles, and authors should consult their funding agency guidelines for details. Registration is easy and free; for further information, see http://orcid.org/.

Dr. Christian Wölke Dr. Diddo Diddens Bastian Heidrich Prof. Dr. Martin Winter

Dr. Isidora Cekic-Laskovic http://orcid.org/0000-0003-1116-1574